

MAXimum-entropy ReconSTRUCTION (MARS): A New Strong-lensing Reconstruction Algorithm for the JWST Era

Sangjun Cha¹  and M. James Jee^{1,2}

¹Department of Astronomy, Yonsei University, 50 Yonsei-ro, Seoul 03722, Korea.
email: sang6199@yonsei.ac.kr

²Department of Physics and Astronomy, University of California, Davis, One Shields Avenue,
Davis, CA 95616, USA

Abstract. The MAXimum-entropy ReconSTRUCTION (MARS) method is a free-form strong-lensing (SL) reconstruction algorithm, which adopts the maximum cross-entropy as a regularization. MARS shows remarkable convergence of multiple images in both source ($\sim 0.''02$) and image planes ($\sim 0.''05 - 0.''1$) while suppressing spurious fluctuations. Although the reconstruction requires a large number of free parameters exceeding $\sim 19,000$, our implementation through PyTorch can obtain the reconstruction within hours. From our test using the publicly available synthetic clusters, we have verified that the reconstructed radial mass profiles are consistent with the truth within 1 percent. This makes MARS one of the best-performing SL reconstruction methods. We apply MARS to the six Hubble Frontier Fields clusters and present new mass reconstruction results. We also reconstruct a mass model of Abell 2744 using both weak-lensing (WL) and SL data from the JWST observations, with the largest dataset of Abell 2744, including 286 SL multiple images and ~ 350 arcmin⁻² WL constraints.

Keywords. Dark matter distribution, Galaxy clusters, Weak gravitational lensing, Strong gravitational lensing

1. Introduction

Thanks to its advantage of not requiring any dynamical assumptions, gravitational lensing is one of the most powerful methods for reconstructing the mass distributions of astronomical objects (Bartelmann & Schneider 2001). Gravitational lensing is usually classified into two types: strong lensing (SL) and weak lensing (WL). WL uses the shape distortion of background galaxies and can provide mass maps for a wide area. SL utilizes the locations of multiply-lensed galaxies and enables us to reconstruct the precise mass distribution around cluster centers (Kneib & Natarajan 2011).

In this study, we reconstruct SL lens models for six galaxy clusters in the Hubble Frontier Fields (HFF) programs by employing a free-form lens modeling algorithm, MARS, which adopts the maximum cross-entropy as a regularization (Cha & Jee 2022, 2023). MARS has shown one of the best performances among various lens modeling algorithms (Cha & Jee 2022), evaluated using the synthetic galaxy clusters Ares and Hera (Meneghetti et al. 2017). For the galaxy cluster Abell 2744 (A2744), one of the targets of the HFF program, we simultaneously reconstruct a mass model using WL and SL data from the JWST observations, including 286 SL multiple images and ~ 350 arcmin⁻² WL constraints. This dataset is the largest ever used for cluster mass reconstruction.

2. Data

For the SL modeling of the HFF clusters, we adopt the multiple image catalogs in Cha & Jee (2023), which compile multiple images from the literature. These multiple images are classified into two classes: gold and silver. Images with spectroscopic redshifts are considered gold images, while those with only photometric redshifts are categorized as silver images. Additionally, images agreed to be lensed by multiple previous studies are also considered silver images. We treat their redshifts as free parameters for the mass reconstruction process. Each cluster has 100 – 200 multiple images, and all of them are converged in both source and lens planes.

By utilizing the publicly available NIRC*am* mosaic images processed by the UNCOVER team† (Bezanson et al. 2022; Weaver et al. 2023), we can reconstruct the mass distribution of A2744 over a wider field than that covered by the HFF program ($\sim 2 \text{ Mpc} \times 2 \text{ Mpc}$ region). We adopt the SL catalog from Cha & Jee (2023) for the region where the HFF data covers. For other regions, we compiled multiple images from Furtak et al. (2023) and Bergamini et al. (2023). Moreover, we identified 16 new multiple-image candidates from 6 systems. WL background sources are extracted based on photometric redshifts provided by the UNCOVER team. We measure the shapes of the sources using the F200W filter from JWST. The final dataset consists of 286 SL multiple images, and the WL source density reaches $\sim 350 \text{ arcmin}^{-2}$, which is the largest dataset ever used for cluster mass reconstruction.

3. Result

Figure 1 displays the reconstructed mass maps of the HFF clusters. Although the MARS algorithm is entirely blind to the locations of the cluster galaxies, the reconstructed mass maps are highly consistent with their locations, while producing small scatters of the multiple images in both the source ($\sim 0.''02$) and the image ($\sim 0.''1$) planes. The lens plane scatters from MARS are lower than the previous results by a factor of 5-10 (see Figure 2). The most impressive case is MACS J0416.1-2403, which has 236 multiple images, all with spectroscopic redshifts. MARS converges its multiple images with small scatters in the image plane ($\sim 0.''084$) while reconstructing a smooth mass map, effectively suppressing spurious fluctuations. For more details, we refer readers to Cha & Jee (2023).

Figure 3 shows the reconstructed mass distribution of A2744 using both WL and SL datasets from JWST. Similar to the HFF clusters, MARS successfully traces the brightest cluster galaxies (BCGs) with the five strongest mass peaks. Not only for the BCGs, but the resulting mass map also shows good agreement with the number and luminosity density of the cluster member galaxies. Furthermore, the mass elongations in the outskirts align consistently with the directions reported for the large-scale filamentary structures observed in the X-ray hot gas (Eckert et al. 2015).

4. Conclusion

We have presented new mass maps of the HFF clusters using the MARS algorithm. Especially for A2744, we ran the mass modeling using both WL and SL datasets from JWST, which are the largest datasets ever used for cluster mass reconstruction. Although MARS is entirely blind to the locations of cluster member galaxies, the resulting mass model successfully traces the locations of BCGs. Moreover, even with more than $\sim 19,000$ free parameters to minimize, the MARS models exhibit excellent convergence in both source and image planes while effectively suppressing spurious fluctuations. By incorporating the WL dataset for mass reconstruction, MARS can predict the mass distribution not only

† <https://jwst-uncover.github.io/DR1.html>

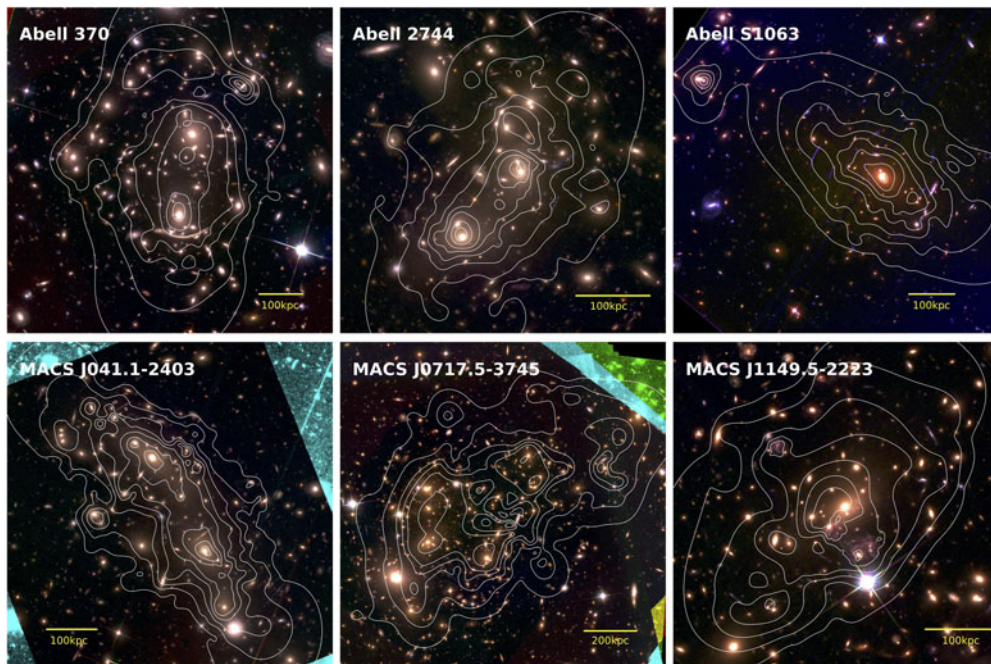


Figure 1. Mass contours of the HFF clusters overlaid on the color composite images. The white contours indicate the convergence κ . The color composite images are generated with the F606W, F814W, and F105W filters for the blue, green, and red channels, respectively except for Abell S1063. The color composite image of Abell S1063 is created with the F435W, F606W, and F814W filters for the blue, green, and red channels, respectively.

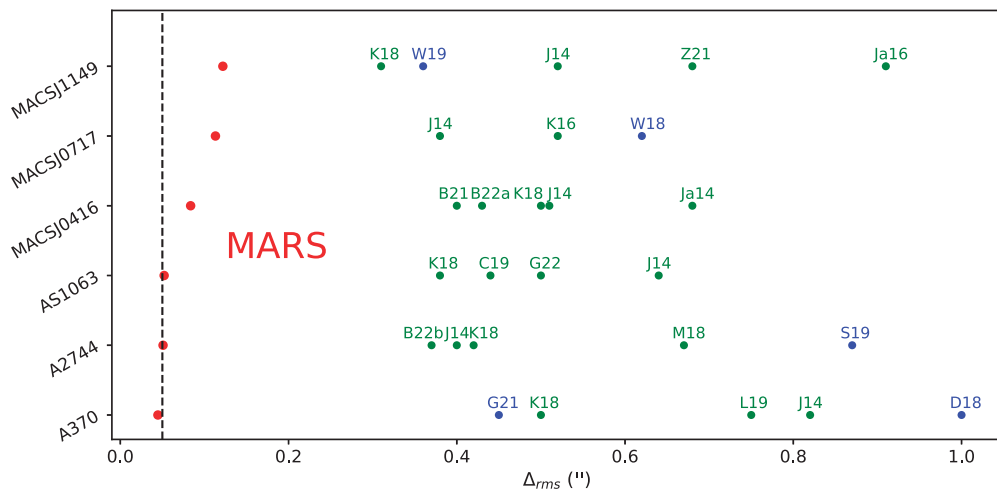


Figure 2. Image plane scatter comparison between MARS and the literature. The green (blue) dots indicate the RMS from the parametric (free-form) methods. The red dots show the RMS from MARS. The black dashed line represents an RMS value of 0."05.

in the region around BCGs but also in the outskirts where there are no SL multiple images. In the current JWST era, with forthcoming observations expected to increase the dataset volumes of both SL and WL, a highly flexible and solidly regularized free-form modeling method like MARS would become a powerful tool to figure out precise mass

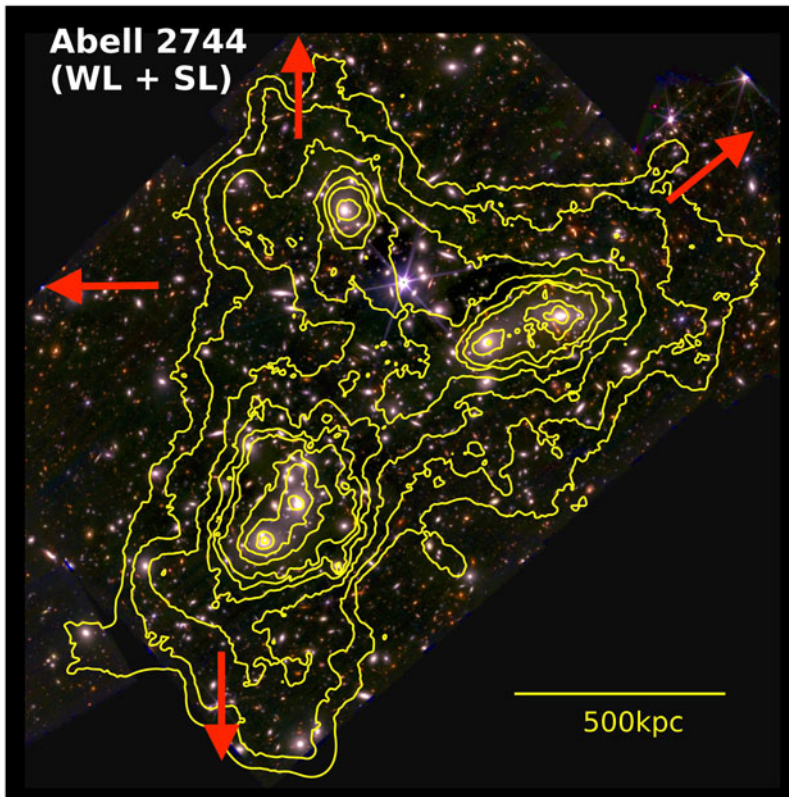


Figure 3. Reconstructed mass contours of A2744 overlaid on the color-composite image. The yellow contours are derived from the mass map using both WL and SL datasets. The red arrows indicate the reported directions of extended filaments observed in the X-ray hot gas. The color composite image is created using the F444W filter for red, the F277W filter for green, and the F115W filter for blue. The FOV is $400'' \times 400''$.

distributions of galaxy clusters across wide fields, from the central region to the outskirts and even beyond the virial radius.

Supplementary material

To view supplementary material for this article, please visit <http://dx.doi.org/10.1017/S1743921323004015>.

References

- Bartelmann, M., & Schneider, P. 2001, *PhR*, 340, 291
 Bergamini, P., Acebron, A., Grillo, E., *et al.* 2023, *ApJ*, 952, 84
 Bezanson, R., Labbe, I., Whitaker, K. E., *et al.* 2022, arXiv:2212.04026
 Cha, S., & Jee, M. J. 2022, *ApJ*, 931, 127
 Cha, S., & Jee, M. J. 2023, *ApJ*, 951, 140
 Eckert, D., Jauzac, M., Shan, H., *et al.* 2015, *Nature*, 528, 105
 Furtak, L. J., Zitrin, A., Weaver, J. R., *et al.* 2023, *MNRAS*, 523, 4568
 Kenib, J. -P., & Natarajan, P. 2011, *A&ARv*, 19, 47
 Meneghetti, M., Natarajan, P., Coe, D., *et al.* 2017, *MNRAS*, 483, 195
 Weaver, J. R., Cutler, S. E., Pan, R., *et al.* 2023, arXiv:2301.02671